Nanoindentation Study of Phase-pure Highly Crystalline Hydroxyapatite Coatings Deposited by Microplasma Spraying

Arjun Dey[1,*] and Anoop Kumar Mukhopadhyay[2]

[1]*Thermal Systems Group, ISRO Satellite Centre, Indian Space Research Organisation, Vimanapura Post, Bangalore-560017, India*

[2]*Advance Mechanical and Materials Characterization Division, CSIR - Central Glass and Ceramic Research Institute, Jadavpur, Kolkata-700032, India*

Abstract: The present contribution has originated from a critical biomedical engineering issue e.g., loosening of metallic prostheses fixed with poly(methylmethylacrylate) (PMMA) bone cement especially in the case of hip joint replacement which ultimately forces the patient to undergo a revision surgery. Subsequently surgeons invented a cementless fixation technology introducing a bioactive hydroxyapatite (HAp) coating to the metallic implant surface. A wide variety of different coating methods have been developed to make the HAp coating on metallic implants more reliable; of which ultimately the plasma spraying method has been commercially accepted. However, the story was not yet finished at all, as many questions were raised regarding coating adherence, stability and bio-functionality in both *in vitro* and *in vivo* environments. Moreover, it has been now realized that the conventional high power plasma spraying (i.e. conventional atmospheric plasma spraying, CAPS) coating method creates many disadvantages in terms of phase impurity; reduced porosity limiting osseointegration and residual stresses which ultimately lead to inadequate mechanical properties and delamination of the coating. Further, poor crystallinity of HAp deposited by CAPS accelerates the rate of bioresorption, which may cause poor adhesion due to quick mass loss of HAp coatings. Therefore, in the present work a very recently developed method e.g., low power microplasma spraying method was utilized to coat HAp on SS316L substrates to minimize the aforementioned problems associated with commercial CAPS HAp coatings. Surgical grade SS316L has been chosen as the substrate material because it is more cost effective than Ti6Al4V and CoCrMo alloys.

INTRODUCTION

A short acronym for Hydroxyapatite is HAp. It has many applications. One of the major applications is as a coating. The coatings are usually porous, but can be made dense also if the end application deserves that. However, the porous coatings are usually deposited on metallic bio-medical implants. The pores in the coating have an important advantage to offer in fact. What happens is that the tissues related to growth of the bone can indeed grow and pass through such pores present in the microstructure of the characteristically porous and heterogeneous HAp coatings.

There are in fact many methods to develop HAp coatings. However, speaking on a commercially popular choice the most accepted method is usage of a plasma spray process. Now, HAp is basically a ceramic material. Characteristically, ceramics have high melting temperature. So, to melt them a high heat flux is required. Eventually, in the case of plasma

spraying process this heat flux will then have to be provided by a plasmatron which generates the plasma torch. Thus, a relatively higher magnitude of plasmatron power is the obvious choice. So, a typical plamatron power of more than e.g., 10,000 W is typically preferred in so far as efficiency optimization of a commercial plasma spraying process is concerned. Such a technical process is popularly known as the conventional atmospheric plasma spraying (CAPS) technique. In other words it needs to be emphasized that as far as a comparison of different practicable and feasible techniques of HAp coating is concerned, the CAPS method enjoys the highest popularity among the manufactures.

Nevertheless, there are two major issues of great concern in such plasma spraying of HAp. The first one is that the high temperature of the plasma jet almost certainly leads to formation of many undesirable phases such as tricalcium phosphate (TCP), tetracalcium phosphate (TTCP) and even CaO. There is also another phase e.g., amorphous calcium phosphate (ACP). ACP is an important contributor to bioactivity as its easy dissolution *in vivo* provides calcium and phosphorus ions required to form bone-like apatite. However, since it is formed close to the interface with the metallic substrate owing to rapid quenching of the molten

*Address correspondence to the author at the Thermal Systems Group, ISRO Satellite Centre, Indian Space Research Organisation, Vimanapura Post, Bangalore-560017, India; E-mails: arjundey@isac.gov.in; arjun_dey@rediffmail.com

particles, its early dissolution may compromise the adhesion of the coating layer to the substrate. This is the reason why the CAPS-HAp coatings with crystallinity well below 70% face severe problem in terms of their *in vivo* stability [1]. It is this particular aspect that primarily led to the origin of the microplasma spraying process (MIPS) that utilizes a plasmatron power (e.g., 1-4 kW) much below that (e.g., 10-40 kW) used to deposit the CAPS-HAp coatings. However, it can still provide both the degree of crystallinity and the degree of phase purity much higher than those values obtained for CAPS-HAp coatings [2]. However, very high crystallinity is not always desired as it renders the HAp bioinert, i.e., a certain amount of easily soluble Ca-P phases must be present for its biological function to occur. In contrast, very poor crystallinity accelerates the rate of bioresorption, which might cause poor adhesion with the substrate due to very quick mass loss of HAp Ca-P phase, especially, for long-term implantation. Therefore, a proper mixture of crystalline and amorphous phases should be present in the Ca-P to get an appropriate bioresorption. In the current research efforts (Ref. [2-9]), MIPS-HAp coatings were deposited on SS316L substrates using a plasmatron with low power of 1.2 kW.

MATERIALS AND METHODS

In-house Synthesis of HAp Powder

The required HAp powder was prepared in our laboratory by controlled addition of orthophosphoric acid (H_3PO_4) to a solution of calcium hydroxide. It is well known that the corresponding formula is given by $Ca(OH)_2$. As the reaction proceeds between calcium hydroxide and orthophosphoric acid added in a desired, well controlled fashion, what this leads to is the precipitation [6,7] of the hydroxyapatite phase in solution with water (H_2O) as a byproduct of the reaction. It is well known [6, 7] that the technical formula for the HAp phase is, e.g., $Ca_{10}(PO_4)_6(OH)_2$. Written explicitly as a chemical reaction equation the reaction implies that ten molecules of calcium hydroxide react with six molecules of orthophophsoric acid, and assuming that a complete reaction of the two reactants happen the end product becomes one molecule of $Ca_{10}(PO_4)_6(OH)_2$ along with eighteen molecules of water (H_2O).

$$10\ Ca(OH)_2 + 6H_3PO_4 = Ca_{10}(PO_4)_6(OH)_2 + 18H_2O \qquad (1)$$
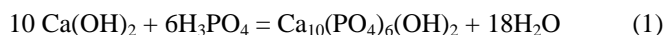
The precipitated HAp particles were designed to have a desired size range. Therefore, the reaction kinetics had to be slowed down. This required a drop-by-drop addition of the aqueous H_3PO_4 solution to the preheated aqueous solution of the corresponding metallic hydroxide which in this particular occasion is e.g., $Ca(OH)_2$. There are two very important characteristics of this particular solution that is most desirable to be preserved during the time the reaction is allowed to occur. The first one is of course the pH of the solution. The pH value of a solution is nothing but the negative logarithm of hydrogen ion concentration in a given solution, for example, it may be mentioned that in our own experiments a pH value of about 11.5 was found [6] to be the most desirable value that leads to high yield for the given particular reaction of calcium hydroxide with orthophosphoric acid as mentioned above. A thermostat was used to keep the $Ca(OH)_2$ solution at a temperature of $\sim$

80^0C. As the drops of the aqueous H_3PO_4 solution started to react with the $Ca(OH)_2$ solution, a whitish precipitate started to be formed [10]. The precipitate was aged for an optimum period. The precipitated whitish powder was sintered in the range of 1240-1260^0C. It was found that the optimum temperature for phase-pure HAp powder synthesis was close to $\sim 1250^0C$ [6,7]. The HAp powder prepared as mentioned above did not possess the characteristic free flowability required for use of the powder feeder of the plasma processing unit. Thus, the largest technical challenge is not only to prepare phase-pure HAp powder but also to prepare a free flowable HAp powder at the same time [8]. It is for this reason that the sintered HAp bulk mass was put through a conventional crusher. The outputs received from the crusher were passed through sieves of different size fractions. This step was found to be of critical importance to obtain eventually a free flowing powder suitable for the MIPS process. To give a visual idea of the different stages involved in the production of the free flowable phase-pure HAp powder synthesis, a typical process flow diagram is presented in Fig. (**1**) [9]. The powder had stoichiometric composition e.g., Ca/P of ~ 1.67 and had a flowability of $\sim 0.5 g \cdot sec^{-1}$ [7]. The particle size distribution shown in Fig. (**2**) revealed a d_{50} of ~ 67 μm [7, 9].
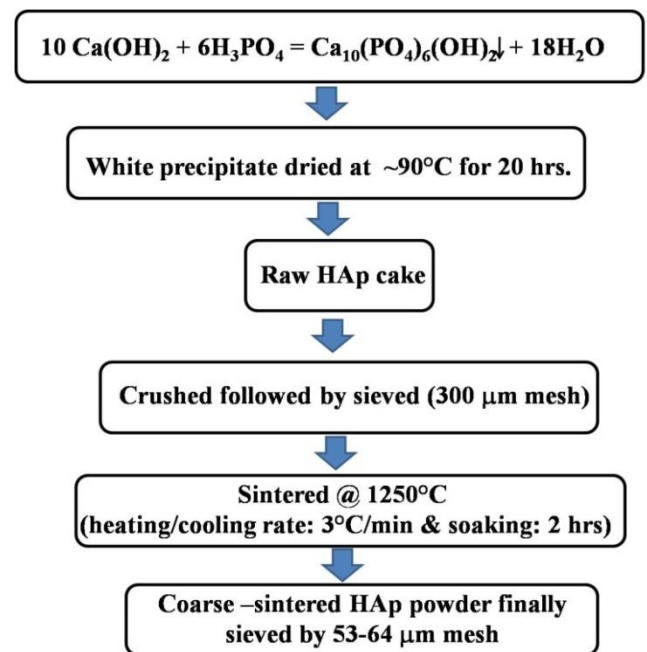
Fig. (1). A typical flow diagram for production of HAp powder suitable for the MIPS process [9].

Deposition of HAp Coatings

The most common type of surgical grade biometallic substrate is 316L stainless steel. This is easily available from commercial vendors. So, this material was chosen as a substrate material for coating deposition in the present work. However, some pre-treatments were necessary prior to deposition. The first of these steps was grit blasting. To achieve this, the SS316L were at first grit blasted with 0.2 mm alumina grit to an average roughness $R_a \sim 2.5$ μm and subsequently cleaned with AR grade acetone in an ultrasonic

Table 1.   Optimized process parameters [9].

Parameters	Values
Gas pressure (primary, in bar)	4
Gas pressure (secondary, in bar)	4
Flow rate (primary, in 10^3 SCCPM)	10
Flow rate (secondary, in 10^3 SCCPM)	20
Powder deposition rate (mg.sec^{-1})	~1.5
Powder size (μm)	-53+64
Input current (Amp)	~ 40
Input voltage (V)	~ 30
Plasmatron power (kW)	1.2
Stand-off distance, SOD (mm)	75
Speed at which sample rotates (rpm)	150
Gap of cathode from plasma nozzle (mm)	1.7
Gap of anode from plasma nozzle (mm)	1

SCCPM: standard cubic centimeters per minute, rpm: rotation per minute

Fig. (2). The particle size distribution of in-house synthesized HAp powder [9].

cleaner, prior to cutting into strips and cylinders of sizes (155 x 20 x 2 mm^3) and (D = 25 mm, L = 25.4 mm), respectively.

A plasmatron unit powered with 1.2 kW was used for MIPS-HAp coating deposition on these substrates. The powder was fed from an external unit associated to the main unit. The unit steps and the necessary details of the MIPS process is elaborated in illustration presented in Fig. (**3**) [9]. The basic working principle of MIPS remains the same as in the case of CAPS process.

A large number of process parameters were needed to be taken care of and simultaneously optimized (Table **1**), to obtain the conditions conducive for the desired quality of the MIPS-HAp coatings developed in the present work. A post-MIPS heat treatment at ~600^{0}C was necessary to enhance the
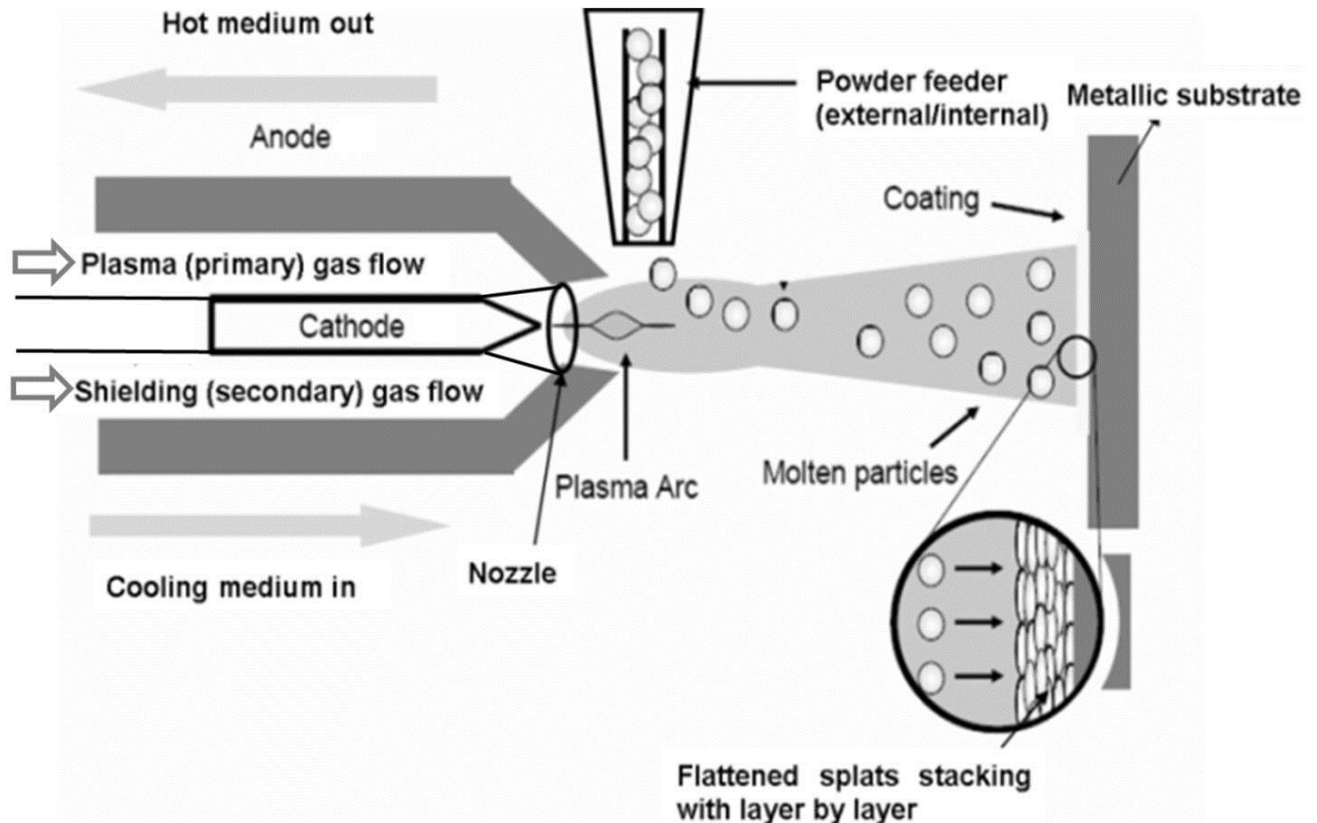
Fig. (3). Schematic of the MIPS process [9].

crystallinity and thereby the bond strength of the coatings. The heating rate was 30°C·min^{-1} during post-depositional heat treatment. The annealing time was 120 minutes. The temperature of annealing was deliberately kept at 600°C. The rate of cooling was chosen to be just equal to the rate of heating such as to avoid any unnecessary imbalance. It is also important to understand whether there is an influence of such a heat treatment on the mechanical properties of the SS316L substrates. Research conducted by Downey II *et al.* [10] had already shown that even when SS316L was kept for a period of as high as 100 hrs at 700°C, the change in strength was insignificant. However, a small variation of hardness was reported for SS316L heat-treated at 700°C and 800°C [11]. Thus, it was decided in the present work to keep the post-depositional heat treatment temperature of the MIPS coatings at 600°C, which is definitely much lower than 700°C or 800°C. Therefore, it may plausibly be argued that at such a low temperature of post-depositional heat treatment chosen in the present work, there would not be any significant effect on the mechanical properties of the SS316L substrates.

Phase Analysis and Microstructural Characterizations

The phase composition of the starting powder and subsequently developed coating were investigated by the conventional X-ray diffraction (XRD) technique. A commercial diffractometer was utilized for this purpose. The particular variant is conventionally known by a trade name called X'pert Pro MPD diffractometer. It was provided by a commercial vendor (e.g., PANalytical, The Netherlands). The diffractometer was operated at 40 kV with the corresponding current of 35 mA. In particular, the well known CuKα_1 line was utilized because it is practically the best monochromatic beam that can be used.

The microstructure of the coating was far from homogeneous, rather, it was highly heterogeneous and hence very challenging to characterize. Help was therefore taken from the well established technique, e.g., scanning electron microscopy (SEM), mostly in secondary electron mode but occasionally also in back scattered electron mode that provides microstructural details particularly for heterogeneous structures full of cracks, intra- and inter-splat pores, unmelted particles etc. This required exploitation of a model s430i electron microscope supplied by Leo, UK.

Bonding Strength Measurement

The ASTM-C633 standard was followed to measure the bonding strength of the coating.

The substrates used for the deposition of the MIPS-HAp coatings were cylindrical in shape. They comprised of a commercially available surgical grade stainless steel, namely SS316L as mentioned earlier. The substrates of about 25 mm diameter were machined from stocks of this material, and subsequently surface finished as stated earlier.

The joining of a coated stub was a challenging task that had to be undertaken. It was found out that adhesive tapes can be very handy in achieving the same. As a typical

illustrative example, but not necessarily limited to, it may be mentioned that an adhesive FM1000 film was utilized for the purpose of joining. Although, this particular variety is a commercial product made available by a manufacturer e.g., Cytec Industries Inc., New Jersey, USA but it must be emphasized that many other equivalently efficient varieties may be obtainable from suppliers of such materials distributed all over the globe.

The tape is generally known to be manufactured as a mixture of two compounds. One of them is polyimide. The other is an epoxy resin. To conduct the tests, mounting of the stubs was necessary. An appropriate fixture was designed in such a fashion in such a way that the stubs could be snugly fitted into it. The next important step was curing. It was done in an air oven. After a few trial and error experiments a temperature of about 300ºC was identified as the appropriate temperature which could initiate curing. However, it was not before a period of as long as 300 minutes that the curing could be claimed as complete to the optimum degree as well as just sufficient. A commercially available universal testing machine was exploited to conduct the tensile tests. The particular model used in our work was 5500R supplied by Instron, USA. The rate of movement for the cross head of the machine was deliberately kept at a low magnitude. To give a typical idea the speed was e.g., as low as about 100 μm per time slot of 60 seconds. All experiments were conducted under usual laboratory ambience in air at room temperature. From the results of these tensile tests the load at which the coating failed were noted. These are then taken as the critical failure load. These data were then converted to bonding strength. The evaluation of the same required a division of the critical failure load data by the corresponding data on contact area that had borne the load.

At least ten individual tensile strength tests were conducted to obtain a representative magnitude of what can be termed as the average value of bonding strength for the current coatings.

Nano-mechanical Characterization

The nanoindentation experiments were performed in the "z" direction. This direction was chosen in such a way that splat orientation remained perpendicular to the "z" direction. Thus, these experiments basically evaluated two local mechanical properties. The first is the nano-hardness (H). The second one is the Young's modulus (E). A plan section of HAp coating was used for this purpose. Prior to the experiments, the samples were mirror polished. A commercial machine, e.g., a standard nanoindenter (Fischerscope) was used for this purpose. The machine had the capability to measure depth with a resolution of 1nm. It had the additional capability to measure force with a resolution of 0.2 μN. The machine was calibrated with nanoindentation measurements made under specified conditions on a standard reference Schott BK7 glass block with calibrated H of 4.14± 0.05 GPa and E of 84.6 ± 1.07 GPa. The calibration data was always checked before each experiment to ensure both accuracy and repeatability of the experimentally measured data. The nanoindentations were placed on the plan section. The range of load used for these experiments covered a span as wide as 10 to 1000 mN. Out

of this load range nine particular magnitudes were chosen as to cover low, intermediate and higher ranges applied on the corresponding Berkovich indenter used for the nanoindentation experiments. The semi-apex angle of the Berkovich indenter was about 65.3^0. Similarly, the tip radius of the Berkovich indenter was small enough e.g., ~150 nm. Since the coating had about 200 µm thickness, the maximum depth of penetration had to be kept within 10% of the same, so that unnecessary contribution of the mechanical properties of the substrate on the data measured for the coating [12] can be avoided. That way, the limiting depth of penetration was 20 µm. In reality, however, the maximum depth of penetration did not exceed even 5 µm which was no doubt well below the limiting value mentioned above. The time to reach effectively insignificant load from the peak load was kept the same as the loading time, e.g., 30 seconds taken to reach the peak load. The coating had two characteristic features inherently present in its microstructure. The first is that it was porous. The second is that it was heterogeneous. For any given load five different locations were chosen randomly on the coating. At each of these locations, a minimum of at least fifteen nanoindentations had been deliberately placed choosing the locations again as randomly as possible. The whole idea behind this exercise was to take care of the inherent heterogeneity of the microstructure of the coating that was expected to be reflected in the resultant data and it did. A particular standard called DIN 50359-1 standard was followed in these measurements of the corresponding H and E values. The load versus depth of penetration plots were exploited for this purpose utilizing one of the models that is globally the most accepted so far. The model is in fact none other than the Oliver and Pharr (O-P) model [13].

Tip area calibration was performed on fused quartz with known modulus. A non-linear sixth order polynomial curve to fit contact area vs. contact depth was generated by the software provided by the nanoindenter. Ideally, this curve should be smooth and of parabolic shape with no inflections. The first order constant, i.e. the C_0 value should always be as close as possible to 24.5 for a Berkovich indentation applied in the present work. Details of the calibration procedure have been already published elsewhere [14].

Prior to nanoindentation, the samples were polished by subsequent application of different grades of diamond pastes (Eastern Diamond Product Ltd., Kolkata, India). An automated polishing machine (Labopol-3, Struers, Denmark) was used. Initially, a coarse polishing was done on a conventional polishing felt with a diamond paste of 20 µm grit size. Subsequently, diamond pastes of comparatively less coarser sizes, e.g. 15, 9 and 6 µm grit sizes were used to cut down the asperity size distribution to a lower average surface roughness value. At each stage, several hours had to be spent followed by inspection with an optical microscope (GX 51, Olympus, USA). After these stages, the fine polishing was continued with diamond pastes of successively finer sizes, e.g. 3 and 1 µm grit sizes. Once the desired low value of surface roughness was achieved, e.g., R_a~1 µm, the final polishing was done with 0.25 µm grit size diamond paste. The final stage of the microstructural relief was obtained after polishing with a fine silica suspension that typically leads to a R_a~0.5 µm.

Further, to evaluate the plain strain fracture toughness the same nanoindentation machine and the same indenter mentioned above were used. The plain strain fracture toughness is denoted by K_{Ic} as it relates to crack propagation under mode I loading. A mirror polished MIPS-HAp coating was used for evaluation of (K_{1c}) in the present work. The evaluation of (K_{1c}) was achieved through the exploitation of a well known equation:

$$K_{1c} = \alpha \left(\frac{E}{H} \right)^{0.5} \left(\frac{P}{C^{1.5}} \right) \qquad (2)$$

where, P is the applied load and C is the average crack length measured from the center of the nanoindent, and E and H are the Young's modulus and nano-hardness of the coating, respectively. In this relationship, α is a numerical constant. Following the work reported by other researchers [15], the magnitude of α was assumed as 16×10^{-3}.

The nanoindentation tests for K_{Ic} measurement were carried out along the cross sections of the coatings. It was further noticed that for indentation fracture toughness of brittle solids, the relation shown in eq. 2 has been well accepted in several studies [16, 17].

Basically, the model utilized here is the problem of a point load acting normal to the surface of an elastic half-space. This is the well-known Boussinesq's problem [18]. In spite of the characteristic microstructural anisotropy present in the MIPS coating, we simply assume that within the microstructurally small enough volume that is being negotiated by the nanoindentation made with the Berkovich tip with a radius of 150 nm, the coating material is approximately represented by an isotropic, elastic half-space. The stress and displacement solutions to the Boussinesq's problem have been used for development of various fracture mechanics models [16, 17, 19-21], all of which pertain to the cases of glass and ceramics in general. Hence, these models were adapted for brittle coatings used in the present work. Basically, all these models deal with the problem of median vent formation beneath point indenters. Initial efforts [19] showed that for $\nu = 0.25$, the three principal stresses yielded $\sigma_{11} > \sigma_{22} > \sigma_{33}$ nearly everywhere in the field, and that σ_{11} and σ_{33} were well contained within planes of symmetry through the normal load axis. Further, the component σ_{11} was computed to be tensile everywhere while the component σ_{33} was computed to be compressive everywhere. This work established that the tensile component of the point indentation could well have a magnitude sufficient to sustain stable growth of a crack in a brittle material. Later efforts [20] considered that the stress field is almost invariably present underneath the nanoindenter in question. It is not only complex in its characteristics but also elastic-plastic in nature. It was proposed that it can be assumed to have comprised of two components. One is an elastic stress component. However, the other one is a residual stress component. The argument was that the elastic component enhances extension of median crack downward. It was proposed to happen during the loading half cycle. However, this process is reversible. Thus, during unloading the median crack would try to close back on itself. What stops it from actually happening is the residual stress component that renders the final crack shape to be of nearly half penny

configuration. What is the origin of this residual stress component? Its irreversible genesis owes to a simple fact. That may be simply told like that the surrounding matrix is classically still elastic in nature although it tries hard to accommodate the nascent, newly created, hardness impression that is still expanding because it bears the signature of permanent, plastic deformation that was yet to be completed. The resulting plastic zone then provides the crack experience a residual force that acts in a direction that is outward from the center of the nanoindent. Thus, the corresponding stress intensity factor can be shown by a large number of generically similar models [16, 20, 21] to be linked to crack length and characteristic ratio.

This characteristic ratio is given by the quotient (E/H). This would mean that the conducive condition that would support stable crack growth to occur from the three corners of the corresponding nanoindent is realized when the net, resultant effectively active stress intensity factor is equated to the corresponding plain strain fracture toughness K_{1c} measured at the cross section of the present coating, which has a thickness much higher than the corresponding plastic zone size. Here, use is made of the fact that the corresponding strain energy release rate, $G = (1-v^2)K_{1c}^2/E$ and the superposition principle of the stress intensity factors remain valid by virtue of the isotropic, elastic half-space assumption mentioned above.

In the current fracture toughness study, the indentation load was applied in the range of 100-1000 mN where crack can be generated with a size of few microns and the typical lengths of the cracks were usually lesser than the size of splats. Therefore, it can be concluded that the present evaluation of toughness measurement was carried out at the scale of microstructure.

As the microstructure of the MIPS-HAp coating was heterogeneous in nature, the several nanoindents (e.g. more than 100 numbers) made at a given load to get a reliable data scattered with a large statistical variation. Further, the nanoindents were performed only on the solid dense area of the coating in a 'site specific' [3] manner.

RESULTS AND DISCUSSIONS

Characterizations of HAp Powder

Fig. (**4**) shows the typical XRD data of HAp powder which was used at the beginning of the present wok. There was occurrence of small amount of CaO. The powder was phase pure with a crystallinity [22] of ~90% [6,7, 9]. If we critically look into the XRD pattern, it may be certainly noted that formations of either TCP or TTCP could not be detected. Usually, along with CaO these phases occur almost always according to the following equations:

HAp = 3 TCP + CaO + H_2O or HAp = 2 TCP + TTCP + H_2O.   (3)
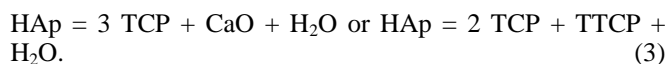
As mentioned earlier, formation of these phases are linked to the dissociation (i.e., incongruent melting) of the HAp powder due to the high sintering temperature of 1250°C [7, 9].

The microstructure had no regular, systematic features (Fig. **5**). However, the average equivalent spherical diameter
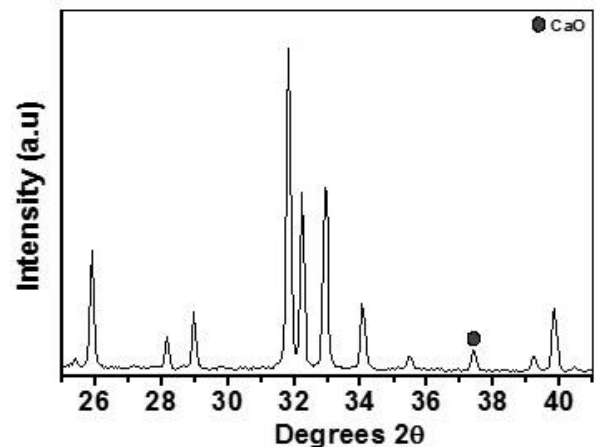
Fig. (4). The XRD pattern of the in-house synthesized HAp powder [9].

was measured by the conventional image analysis technique to be ~65 µm in accord with the result shown in Fig. (**2**).

Characterization of MIPS-HAp Coating

Figs. (**6a** and **b**) show the typical XRD spectra of HAp coatings both in as-sprayed and post-spraying heat-treated conditions, respectively. In the XRD spectra of as-sprayed HAp coatings (Fig. **6a**) there were two minor peaks. One represented crystalline α-TCP. The other represented TTCP. All the other peaks in the as-sprayed MIPS-HAp coatings are characteristic of pure HAp (Fig **6a**). The degree of crystallinity (e.g., ~80%) was slightly below that of the starting powder (~90%) [9,7]. As mentioned earlier, the slight decrease in crystallinity could be linked to formation of either amorphous phase or other crystalline phases. In contrast to this, all the peaks which represent HAp phase formation had occurred in the XRD spectra of the coating following heat-treatment (Fig. **6b**). Most likely due to re-crystallization of the amorphous phase the heat-treated coating had its crystallinity enhanced by ~12% [9].

The heterogeneous microstructure of the MIPS-HAp coatings (Fig. **7**) is presumably suitable for bone tissue in-growth owing to its ~ 50-70 µm size splats with ~10-50 µm macro- and ~1 µm sized micropores [7, 9].
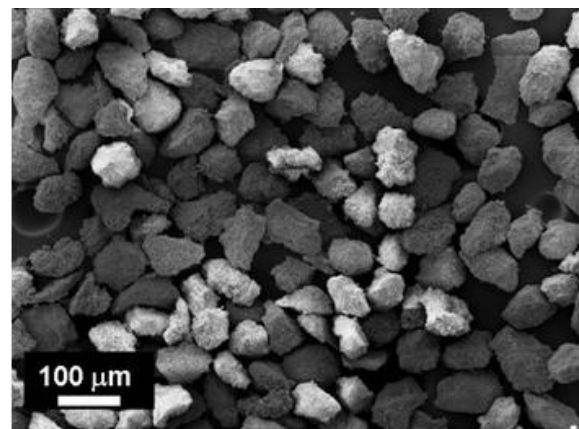
Fig. (5). SEM micrograph of the sintered HAp granules [9].
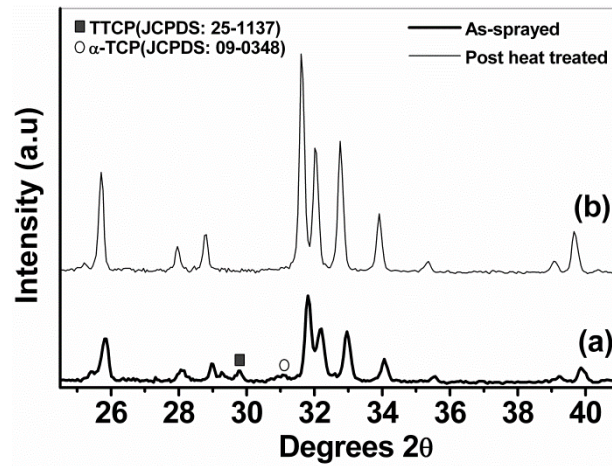
Fig. (6). Typical XRD patterns of MIPS-HAp coating on SS316L: (**a**) as-sprayed and (**b**) post- spraying heat-treated at 600^{0}C [9].

Scanning electron micrographs of mirror-polished surfaces (Fig. 8a) and cross-sections (Fig. 8b) of coatings showed a large number of features such as macrocracks, microcracks, and cracks formed between two adjacent splats. In addition, there were cracks within single splats as well as macro- and micropores. The number of electron microscopy images utilized to measure an average data of a given microstructural feature was not less than at least ten or more.

For the optimized HAp coating (Table **1**) [7, 9] the average open porosity was ~20 vol% and thickness was ~210 ± 6.3 μm. The thickness data suggested that reasonable uniformity was achieved for the coating thickness in the present work. There was an interface between the coating and the substrate. It appeared to be reasonably continuous. There was no obvious sign of any major damage like a crack or a delamination at this interface. However, minor presence of
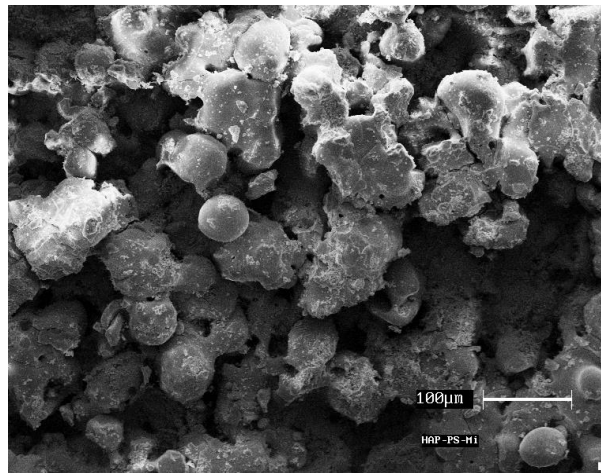
Fig. (7). SEM micrograph of the surface of MIPS-HAp coating in 'as-sprayed' condition [9].
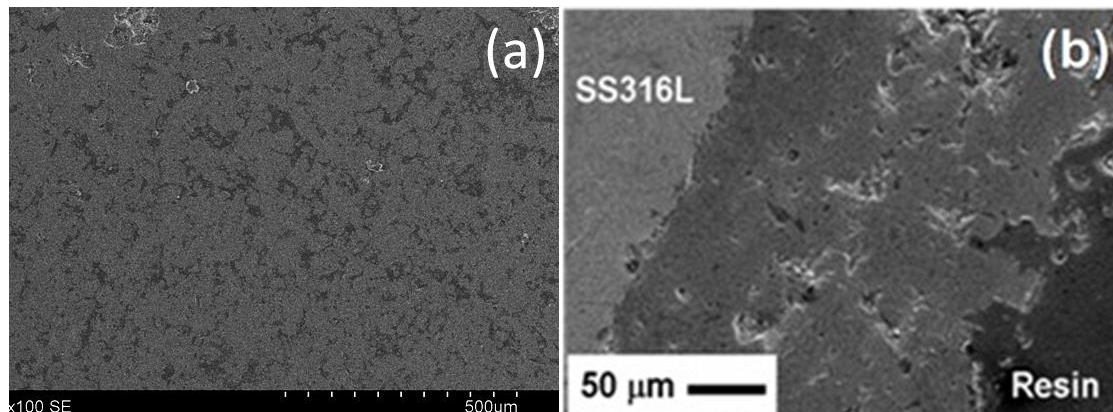
Fig. (8). Micrographs of MIPS-HAp coatings: (**a**) polished surface [9] and (**b**) cross section [3].
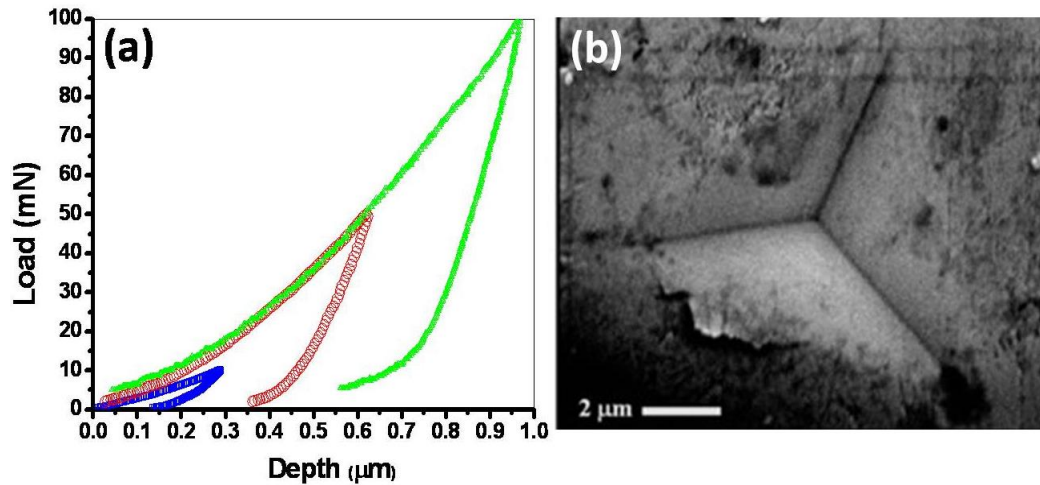
Fig. (9). (**a**) Load-depth plots from nanoindentation experiments at various loads e.g., 10, 50 and 100 mN [9] and (**b**) electron photomicrograph of a typical nanoindent [5] made on the MIPS-HAp coated surface.

some pores and cracks were apparent from the image of the cross-section.

Bonding Strength of MIPS-HAp Coating

MIPS-HAp coating's bonding strength was measured as 12.6 ± 0.31 MPa [6, 9]. The cohesive and adhesive failure modes were both involved in coating failure. Thus, mode of fracture had a rather strong effect on the bonding strength. Cohesive failure may weaken the integrity of the coating layer lamellae and thus contribute to delamination and spalling.

Nano-hardness and Young's Modulus

The data presented in Fig. (**9a**) show the typical load-depth plots from nanoindentation experiments at various loads while the SEM image of a single indent on the coating is shown in Fig. (**9b**). Further, the characteristic values of H (e.g., H_{char}) and E (e.g., E_{char}) for each load were calculated from these data through the application of Weibull statistics [5, 8] and are plotted respectively as a functions of the applied nanoindentation loads in Figs. (**10a** and **10b**).

On the plan section, H_{char} and E_{char} exhibited magnitudes that spanned the range of about 5 to 1.5 GPa and 100 to 63 GPa, respectively, as the load applied during the nanoindentation experiments was increased from 10 to 1000 mN. When the applied nanoindentation load was small enough, e.g., 10 mN, the coating had characteristic value of 5 GPa for nano-hardness at nearly 200 nm depth which degraded to e.g., ~2 GPa for a higher load of 1000 mN at a corresponding depth of about 3000 nm. Thus, apparently there was an indentation size effect (ISE) that was quite evidently reflected in the experimental data. The characteristic value for Young's modulus was 100 GPa and 60 GPa evaluated at 10 mN and 1000 mN loads, respectively [5, 8].

The present hardness and elastic modulus data are well in agreement with the reported data [23, 24], however, they are not one to one comparable with the data reported in literature as the deposition method, microstructure and the measurement methods of hardness and modulus were not same.
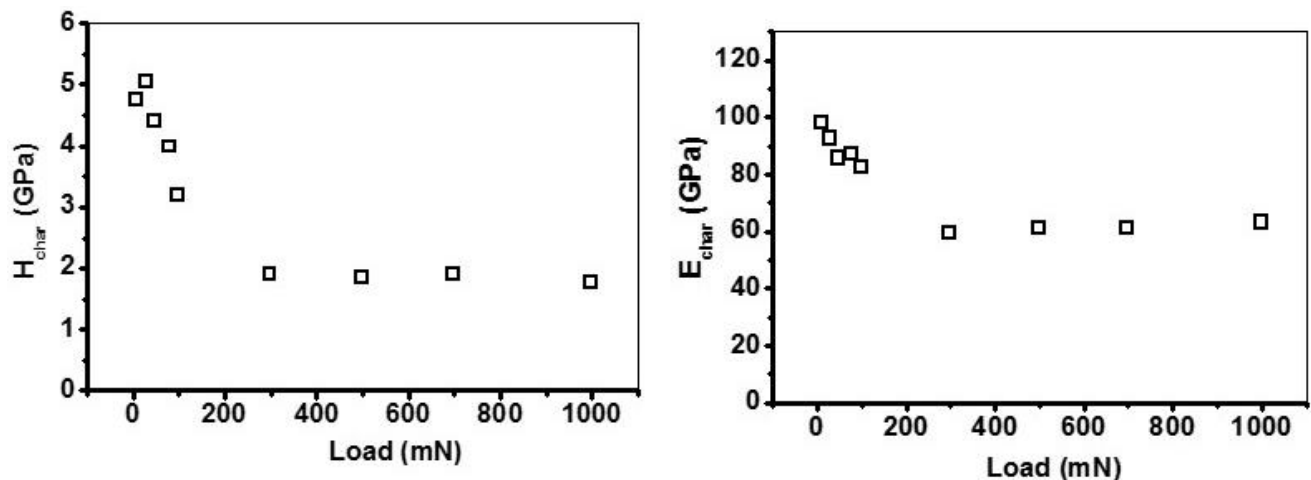
Fig. (10). Influence of indentation loads on variation of (**a**) nano-hardness, H and (**b**) elastic modulus, E of MIPS-HAp coatings [8].

In spite of the high porosity, the MIPS-HAp coatings showed a fracture toughness value of ~0.6 MPa.m$^{0.5}$ measured at a comparatively low load of 100 mN [3]. The literature status of the fracture toughness value of the HAp coatings developed by various thermally sprayed techniques including presently developed MIPS-HAp coating is shown in Fig. (**11**). The present fracture toughness value is comparable to the literature data obtained on dense HAp coatings. In fact, it showed a magnitude marginally higher than the reported value of fracture toughness which was measured for other thermally sprayed coatings with dense microstructure although the direct comparison of the present toughness value with the literature report is not feasible as the microstructure and measurement methods are not equal. Further, as shown in Fig. (**12**) the toughness value was marginally decreased as the indentation load was increased.

CONCLUSION

In the present work, phase-pure highly crystalline hydroxyapatite coatings were developed on 316L grade stainless steel substrates utilizing a novel microplasma spray technique. Subsequently, the MIPS-HAp coatings were characterized in-depth. In spite of having a characteristic heterogeneous microstructure with inter/intra- splat microcracks and ~ 50-70 μm sized macro- and ~1 μm sized micropores, as well as 20 vol.% open porosity, the coatings showed moderate adhesive bond strength of about 13 MPa as well as high nano-hardness (6.19 GPa) and Young's modulus (92.32 GPa). The fracture toughness value was measured as about ~0.6 MPa.m$^{0.5}$ by nanoindentation technique.

CONFLICT OF INTEREST

The authors confirm that this article content has no conflict of interest.
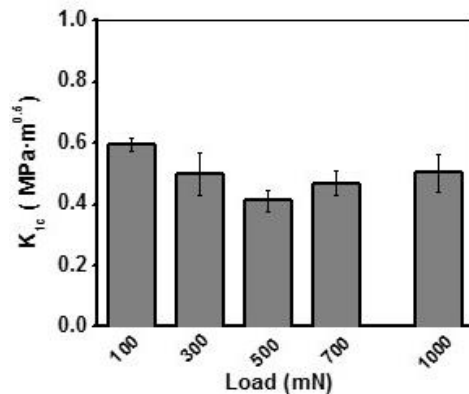
Fig. (12). The variation of fracture toughness of the MIPS-HAp coatings as a function of the applied nanoindentation load [3].

DISCLOSURE

Part of the information included in this chapter has been previously published in Mater. Manufact. Process., 24(12) (2009) 1321-1330; Int. J.Appl. Ceram. Technol., 8(3) (2011) 572-590; Ceram. Int., 35(6)(2009) 2295-2304; J. Mater. Sci., 44 (18) (2009) 4911-4918 and Adv. Appl. Ceram., 109(6) (2010) 346-354.
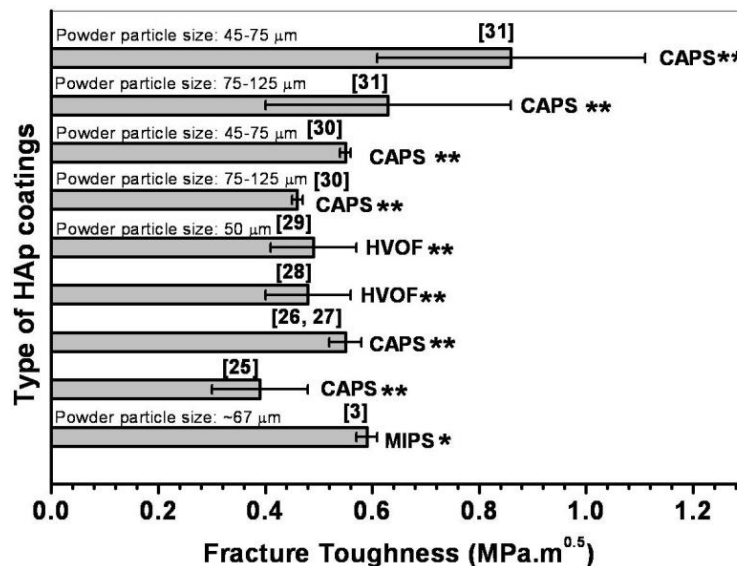
Fig. (11). Literature status of the fracture toughness value of the HAp coatings developed by various thermally sprayed coating techniques [3, 25-31]. CAPS: Conventional atmospheric spraying process, HVOF: High velocity oxy fuel technique and MIPS: Microplasma spraying process, ** Fracture toughness measured by Vicker's microindentation on HAp coatings developed on Ti6Al4V substrate with dense microstructure.* Fracture toughness measured by Berkovich nanoindentation on porous MIPS-HAp coating on SS316L.

REFERENCES

[1]   W. Tong, J. Chen, X. Li, Y. Cao, Z. Yang, J. Feng, X. Zhang, "Effect of particle size on molten states of starting powder and degradation of the relevant plasma-sprayed hydroxyapatite coatings", *Biomaterials*, vol. 17, pp. 1507-1513, 1996.

[2]   A. Dey, S. K. Nandi, B. Kundu, C. Kumar P. Mukherjee, S. Roy, A.K. Mukhopadhyay, M.K. Sinha, D. Basu, "Evaluation of hydroxyapatite and b-tri calcium phosphate microplasma spray coated pin intra-medullarly for bone repair in a rabbit model", *Ceram. Int.*, vol. 8, pp. 1377-1391, 2011.

[3]   A. Dey, A.K. Mukhopadhyay, "Fracture toughness of microplasma sprayed hydroxyapatite coating by nanoindentation", *Int. J. Appl. Ceram. Technol.*, vol. 8, pp. 572-590, 2011.

[4]   A. Dey, A.K. Mukhopadhyay, "Anisotropy in nano-hardness of microplasma sprayed hydroxyapatite coating", *Adv. Appl. Ceram.*, vol. 109, pp. 346-354, 2010.

[5]   A. Dey, A.K. Mukhopadhyay, S. Gangadharan, M.K. Sinha, D. Basu, N.R. Bandyopadhyay, "Nanoindentation study of microplasma sprayed hydroxyapatite coating", *Ceram. Int.*, vol. 35, pp. 2295-2304, 2009.

[6]   A. Dey, A.K. Mukhopadhyay, S. Gangadharan, M.K. Sinha, D. Basu, "Characterization of microplasma sprayed hydroxyapatite coating", *J. Therm. Spray Technol.*, vol. 18, pp. 578-592, 2009.

[7]   A. Dey, A.K. Mukhopadhyay, S. Gangadharan, M.K. Sinha, D. Basu, "Development of hydroxyapatite coating by microplasma spraying", *Mater. Manuf. Proc.*, vol. 24, pp. 1321-1330, 2009.

[8]   A. Dey, A.K. Mukhopadhyay, S. Gangadharan, M.K. Sinha, D. Basu, "Weibull modulus of nano-hardness and elastic modulus of hydroxyapatite coating", *J. Mater. Sci.,* vol. 44, pp. 4911-4918, 2009.

[9]   A. Dey, *"Physico-chemical and mechanical characterization of bioactive ceramic coating"*, PhD Dissertation, Bengal Engineering and Science University, Shibpur, Howrah, India, 2011.

[10]   S. Downey II, P.N. Kalu, K. Han, "The effect of heat treatment on the microstructure stability of modified 316LN stainless steel", *Mater. Sci. Eng. A*, vol. 480, pp. 96-100, 2008.

[11]   S. H. Kang, H. Jina, J. Jang, D.H. Kim, K.H. Oh, D. Foley, X. Zhang, *"In Transactions of the Korean Nuclear Society Autumn Meeting"*, Jeju, Korea, October 21-22, pp. 307-308, 2010.

[12]   P.J. Burnett, D.S. Rickerby, "The mechanical properties of wear-resistant coatings: I: Modelling of hardness behaviour", *Thin Solid Films*, vol. 148, pp. 41-50, 1987.

[13]   W.C. Oliver, G.M. Pharr, "An improved technique for determining hardness and elastic modulus using load and displacement sensing indentation experiments", *J. Mater. Res.*, vol. 7, pp. 1564-1583, 1992.

[14]   A. Dey, A.K. Mukhopadhyay, *"Nanoindentation of brittle solids*, CRC Press/Taylor and Francis Group", 2014.

[15]   X. Guo, J. Gough, P. Xiao, "Electrophoretic deposition of hydroxyapatite coating on Fecralloy and analysis of human osteoblastic cellular response", *J. Biomed. Mater. Res. A*, vol. 80, pp. 24-33, 2007.

[16]   G. R. Anstis, P. Chantikul, B.R. Lawn, D.B. Marshall, "A critical evaluation of indentation techniques for measuring fracture toughness: I, Direct crack measurements", *J. Am. Ceram. Soc.,* vol. 64, pp. 533-538, 1981.

[17]   C.B. Ponton, R.D. Rawlings, "Vickers indentation fracture toughness test. Part 1: Review of literature and formulation of standardised indentation toughness equations", *Mater. Sci. Technol.*, vol. 5, pp. 865-872, 1989.

[18]   C. Atkinson, J.M. Martinez-Esnaola, M.R. Elizalde, "Contact mechanics: a review and some applications", *Mater. Sci. Technol.,* vol. 28, pp. 1079-1091, 2012.

[19]   B.R. Lawn, M.V. Swain, "Microfracture beneath point indentations in brittle solids", *J. Mater. Sci.*, vol. 10, pp. 113-122, 1975.

[20]   B.R. Lawn, A.G. Evans, D.B. Marshall, "Elastic/plastic indentation damage in ceramics: the median/radial crack system", *J. Am. Ceram. Soc.*, vol. 63, pp. 574-581, 1980.

[21]   D.B. Marshall, B.R. Lawn and A.G. Evans, "Elastic-plastic indentation damage in ceramics: the lateral crack system", *J. Am. Ceram. Soc.*, vol. 65, pp. 561-566, 1982.

[22]   E. Landi, A. Tampieri, G. Celotti, S. Sprio, "Densification behaviour and mechanisms of synthetic hydroxyapatites", *J. Eur. Ceram. Soc.*, vol. 20, pp. 2377-2387, 2000.

[23]   T.G. Nieh, A.F. Jankowski, J. Koike, "Processing and characterization of hydroxyapatite coatings on titanium produced by magnetron sputtering", *J. Mater. Res.*, vol. 16, pp. 3238-3245, 2001.

[24]   K.A. Khor, H. Li, P. Cheang, "Characterization of the bone-like apatite precipitated on high velocity oxy-fuel (HVOF) sprayed calcium phosphate deposits", *Biomaterials*, vol. 24, pp. 769-775, 2003.

[25]   K. Balani, R. Anderson, T. Laha, M. Andara, J. Tercero, E. Crumpler, A. Agarwal, "Plasma-sprayed carbon nano tube reinforced hydroxyapatite coatings and their interaction with human osteoblasts *in vitro*", *Biomaterials*, vol. 28, pp. 618-624, 2007.

[26]   L. Fu, K.A. Khor, J.P. Lim, "Yttria stabilized zirconia reinforced hydroxyapatite coatings", *Surf. Coat. Technol.*, vol. 127 pp. 66-75, 2000.

[27]   L. Fu, K.A. Khor, J.P. Lim, "Processing, microstructure and mechanical properties of yttria stabilized zirconia reinforced hydroxyapatite coatings", *Mater. Sci. Eng. A*, vol. 316, pp. 46-51, 2001.

[28]   H. Li, K.A. Khor, P. Cheang, "Titanium dioxide reinforced hydroxyapatite coatings deposited by high velocity oxy-fuel (HVOF) spray", *Biomaterials*, vol. 23, pp. 85-91, 2002.

[29]   H. Li, K.A. Khor, P. Cheang, "Young's modulus and fracture toughness determination of high velocity oxy-fuel-sprayed bioceramic coatings", *Surf. Coat. Technol.*, vol. 155, pp. 21-32, 2002.

[30]   M. Wang, X.Y. Yang, K.A. Khor, Y. Wang, "Preparation and characterization of bioactive monolayer and functionally graded coatings", *J. Mater. Sci. Mater. Med.,* vol. 10, pp. 269-273, 1999.

[31]   S.W.K. Kweh, K.A. Khor, P. Cheang, "Plasma-sprayed hydroxyapatite (HA) coatings with flame-spheroidized feedstock: microstructure and mechanical properties", *Biomaterials*, vol. 21, pp. 1223-1234, 2000.